PAPER

Understanding phase-change materials with unexpectedly low resistance drift for phase-change memories†

Chao Li,[a] Chaoquan Hu, [iD] *[a] Jianbo Wang,[b] Xiao Yu,[a] Zhongbo Yang,[a] Jian Liu,[a] Yuankai Li,[a] Chaobin Bi,[a] Xilin Zhou*[c] and Weitao Zheng [iD] *[ad]

There is an increasing demand for high-density memories with high stability for supercomputers in this big data era. Traditional dynamic random access memory cannot satisfy this requirement due to its limitation of volatile and power-consumable data storage. Multi-level cell phase-change memory (MLC PCM) based on phase-change materials possesses a higher storage density, and is considered to be the most promising candidate. However, a detrimental resistance drift exists commonly in phase-change materials, and it destroys the stability and greatly limits the development of MLC PCM. Here, we propose a completely new strategy to suppress resistance drift by exploring its microscopic mechanism *via* combinations of theoretical calculations and experiments. We have found, for the first time, that resistance drift originates from the change in electron binding energy induced by structural relaxation and is proportional to the reciprocal of the dielectric coefficient according to the hydrogen-like model. On this basis, we propose to reduce the resistance drift by increasing the thermal stability of the dielectric coefficient. Two series of experiments prove the effectiveness of our new strategy. The resistance drift exponent of phase-change films is significantly reduced to 0.023 using our strategy, which is lower by half than the best result (0.050) reported previously. Interestingly, the films also show improved storage properties. These results not only unravel the fact that the stability and storage function of phase-change films can be simultaneously improved by modification of dielectric properties but also pave the way for future material design for stable MLC PCM.

Introduction

With the rise of big data, memories with a higher storage density are required for supercomputers and smart terminals.[1,2] Traditional dynamic random access memory (DRAM) has limited storage density because of its limitation of volatile and power-consumable data storage.[3] Therefore, DRAM cannot meet the requirements of high-performance memory in this big data era. Multi-level cell phase-change memory (MLC PCM) based on phase-change materials has multiple logic states,[4–6] which makes it able to store more than 2 bits per cell and achieve high storage density.[7–11] In addition, the fast reversible switching between amorphous and crystalline states of nonvolatile phase change materials requires an energy of only a few pJ.[12–15] Therefore, MLC PCM not only has a high storage density but also a low energy consumption, which makes it widely regarded as the most promising technology to replace DRAM.[16–19]

To realize MLC technology, the logical states of adjacent levels should be well separated.[20–23] This means that the resistance of the phase-change materials should remain constant over time.[24–26] Unfortunately, it is unstable and this usually increases with time. This phenomenon is called resistance drift, which greatly limits the development of multi-level cell technology.[27–29] Resistance drift can be quantitatively described by the resistance drift exponent ν_R,[30–32] which is calculated by:

$$\nu_R = \frac{\ln\left(\dfrac{R}{R_0}\right)}{\ln\left(\dfrac{t}{t_0}\right)} \tag{1}$$

where R and R_0 are the resistances at t and t_0, respectively. For a $Ge_2Sb_2Te_5$ film, ν_R is about 0.1 at room temperature,[33–35] meaning that its resistance doubles in three hours. This can cause significant problems such as data loss or data-reading

[a] State Key Laboratory of Superhard Materials, Key Laboratory of Automobile Materials of MOE, School of Materials Science and Engineering, Jilin University, Changchun 130012, China. E-mail: cqhu@jlu.edu.cn, wtzheng@jlu.edu.cn

[b] School of Science, Changchun University of Science and Technology, Changchun 130022, China

[c] Max Planck Institute of Microstructure Physics, Weinberg 2, D-06120, Halle (Saale), Germany. E-mail: xilin.zhou@mpi-halle.mpg.de

[d] State Key Laboratory of Automotive Simulation and Control, Jilin University, Changchun 130025, China

† Electronic supplementary information (ESI) available. See DOI: 10.1039/c8tc00222c

This journal is © The Royal Society of Chemistry 2018

J. Mater. Chem. C, 2018, **6**, 3387–3394 | 3387

error and seriously affect the storage function and the reliability of phase-change memory. In magnetoresistive random access memory (MRAM), the resistance drift also leads to data-reading error and is harmful to the reliability of devices.[36] Therefore, it is very important to understand the microscopic origin of resistance drift and propose an effective way to overcome this problem.

Several studies on the microscopic origin of resistance drift have been conducted during the last decade.[37–44] Fantini[35] and Gabardi[44] attributed the resistance drift to the widening of the band gap induced by structural relaxation in GeTe and $Ge_2Sb_2Te_5$ films. However, Cho,[45] Martin[42] and Zipoli[46] argued that the resistance drift originated from the changes in the relative position of the Fermi level. In addition, the effects of composition, doping and cell structure on ν_R have also been investigated. It is shown that the ν_R of GeTe films is significantly influenced by composition[41,43,47] and Sn doping,[40] but it is hardly affected by carbon doping.[39] Koelmans[48] overcame the limitations of traditional device structures by developing projected phase-change memory devices. They filled the area parallel to phase-change materials with projected materials, whose resistance is between those of amorphous and crystalline phases. This new device structure has played an important role in achieving high-density storage and improving the stability of phase-change memory.

Although research studies on the resistance drift in phase-change films have been carried out and some results have been reported, there are still two important problems. First, there is still disagreement concerning the understanding of resistance drift,[35,42,44–46] and the microscopic origin of resistance drift remains vague. Second, the ν_R values of phase-change films have been reported to be about 0.050–0.130,[35,40–42] far greater than the ideal value of 0.010.[49] There has not yet been an effective way to reduce the resistance drift in phase-change films.

In this paper, we explore the microscopic origin of resistance drift in Ge–Sb–Te films and propose a new strategy for reducing resistance drift. A proportional relationship between resistance drift and the reciprocal of the dielectric coefficient has been built for the first time according to the hydrogen-like model. Thus, the resistance drift originates from the change in the dielectric coefficient induced by structural relaxation (Fig. 1a). On the above basis, we propose a completely new strategy to reduce resistance drift in phase-change films: improving the thermal stability of the dielectric coefficient. Two validation experiments prove that the new strategy is very effective. The ν_R of the films is reduced to 0.023, which is lower by half than the best result (0.050) reported in the literature (Fig. 1b). The underlying mechanisms are discussed in detail by combining the theoretical calculations and experiments.

Results and discussion

Resistance drift in amorphous phase-change films is a process wherein the resistance increases with time. In a semiconductor, the resistance (R) is related to the band gap (E_g) according to $R = R_{min} \exp\left(\dfrac{E_g}{k_0 T}\right)$, where R_{min} is the resistance when $E_g = 0$,

k_0 and T are the Boltzmann constant and temperature (Kelvin), respectively. To explore the reason for resistance drift, we measured the sheet resistances and band gaps of $Ge_8Sb_2Te_{11}$ films annealed at 50 °C with different duration times (Fig. 1c). The results show that both the sheet resistance and band gap increase gradually with annealing time. The linear dependence between them (Fig. 1d) indicates that the resistance drift is indeed attributable to the widening of the band gap.

The widening of the band gap means that the electron binding energy increases. According to the hydrogen-like model, the electron binding energy is roughly equal to the Coulomb Potential $U(\mathbf{r})$ of electrons,[50] which can be calculated by:

$$U(\mathbf{r}) = -\frac{e^2}{4\pi\varepsilon_v\varepsilon|\mathbf{r}|} \tag{2}$$

where $\mathbf{r}$ is the position vector of the electron, ε_v and ε are the dielectric coefficients of the vacuum and material, respectively, and e is the charge of an electron. According to this formula, the electron binding energy is proportional to the reciprocal of the dielectric coefficient of the material. To explore the reason for the widening of the band gap, we measured the reciprocal of the dielectric coefficient of the films at different annealing times and the corresponding results are shown in Fig. 1c. The linear relationship between the band gap and the reciprocal of the dielectric coefficient (Fig. 1e) indicates that the widening of the band gap originates from the increase in the reciprocal of the dielectric coefficient.

In a semiconductor material, the dielectric coefficient depends on its polarizability, which is related to the distribution of charges.[51] The amorphous phase-change films are in thermodynamic non-equilibrium. It can return to quasi-equilibrium during annealing due to energy minimization, which is called structural relaxation.[28] In that case, atoms move from the non-equilibrium position to the equilibrium position (Fig. 1a). This was generally attributed to the formation of shorter covalent bonds around Ge atoms during annealing, which effectively suppresses the polarization of atoms and thus reduces the dielectric coefficient.

The relationship between the sheet resistance, the band gap and the reciprocal of the dielectric coefficient (Fig. 1c–e) shows that resistance drift in phase-change films originates from the widening of the band gap, which is attributed to the decrease in the dielectric coefficient and increase in the electronic binding energy caused by structural relaxation. It has been found, for the first time, that the ν_R of phase-change films is proportional to the reciprocal of the dielectric coefficient according to the hydrogen-like model, which will be further demonstrated by the following experiments (Fig. 2).

On the basis of the quantitative relationship between resistance drift and the reciprocal of the dielectric coefficient, we proposed a new strategy to reduce resistance drift in phase-change films: improving the thermal stability of the dielectric coefficient. Since the introduction of point defects and heterogeneous atom doping are effective ways to control the dielectric coefficients of semiconductor materials, we expect that vacancy incorporation and nitrogen doping may improve the thermal stability of

3388 | J. Mater. Chem. C, 2018, 6, 3387–3394

This journal is © The Royal Society of Chemistry 2018
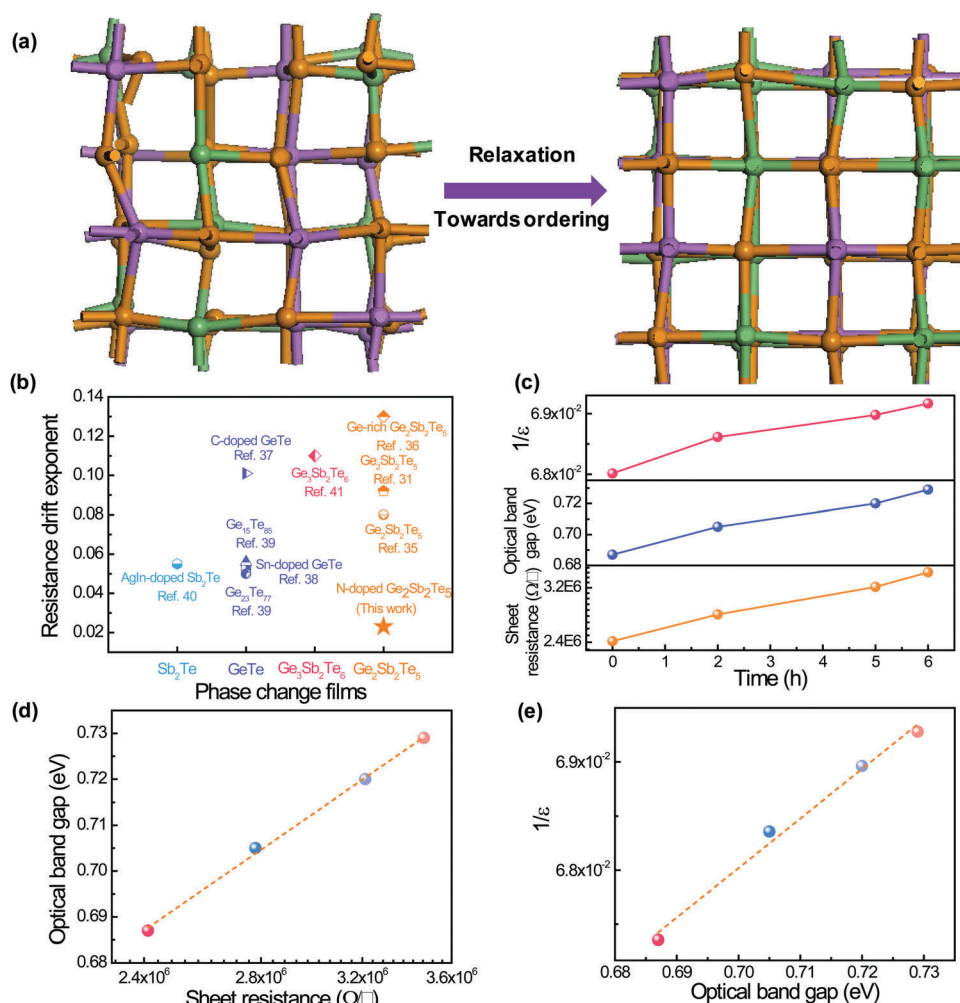
Fig. 1 (a) Structural relaxation causes the change in atomic position and the local structure evolves to a more ordered one. (b) Comparison between the results of other studies and ours. (c) Sheet resistance, band gap and the reciprocal of the dielectric coefficient of $Ge_8Sb_2Te_{11}$ films as functions of annealing time. (d) Linear relationship between the sheet resistance and band gap. (e) Linear relationship between the band gap and the reciprocal of the dielectric coefficient.

the dielectric coefficient of Ge–Sb–Te films and reduce the resistance drift. To verify the feasibility of this strategy, we carried out the following two experiments: (1) changing the Ge, Sb and Te contents in the films to achieve different concentrations of incorporated vacancies (Fig. 2a–c); and (2) introducing N_2 during the preparation process to obtain different contents of doped nitrogen atoms (Fig. 2d–f).

We investigated the effect of annealing on the surface morphology and phase transition. Our atomic force microscopy and scanning electron microscopy measurements (Fig. S1–S4, ESI†) show that there is no significant change in the surface morphologies of the films after annealing at 50 °C. X-ray diffraction and electron diffraction experiments (Fig. S5 and S6, ESI†) demonstrate that there is no amorphous to crystalline phase transition after annealing at 50 °C. These results are in good agreement with previous research studies, indicating that there is no significant change in the morphology and structure of the film during the annealing process.[52,53]

Fig. 2a shows the sheet resistances of the Ge–Sb–Te films with different vacancy concentrations as a function of annealing

time. It can be seen that ν_R decreases from 0.124 to 0.085 as the vacancy concentration increases from 9.1% ($Ge_8Sb_2Te_{11}$) to 20.0% ($Ge_2Sb_2Te_5$). However, when the vacancy concentration increases to 28.6% ($Ge_1Sb_4Te_7$), the ν_R increases to 0.090. This trend indicates that the incorporation of an appropriate amount of vacancies can reduce resistance drift in phase-change films. To quantitatively reveal the relationship between resistance drift and the reciprocal of the dielectric coefficient, a drift exponent of the reciprocal of the dielectric coefficient ($\nu_{1/\varepsilon}$) was defined according to eqn (1). It is calculated using eqn (3). According to this formula, the higher the thermal stability of the dielectric coefficient, the lower the $\nu_{1/\varepsilon}$.

$$\nu_{1/\varepsilon} = \frac{\ln\left(\dfrac{1/\varepsilon}{1/\varepsilon_0}\right)}{\ln\left(\dfrac{t}{t_0}\right)} \tag{3}$$
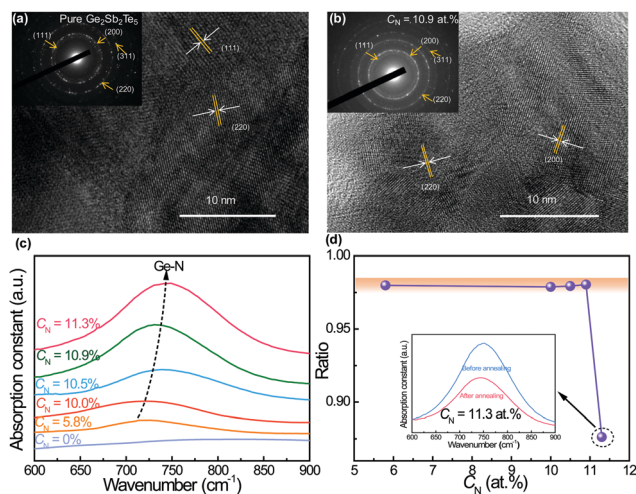
Fig. 2b shows the ν_R and $\nu_{1/\varepsilon}$ of the film as functions of vacancy concentration. The good linear relationship between
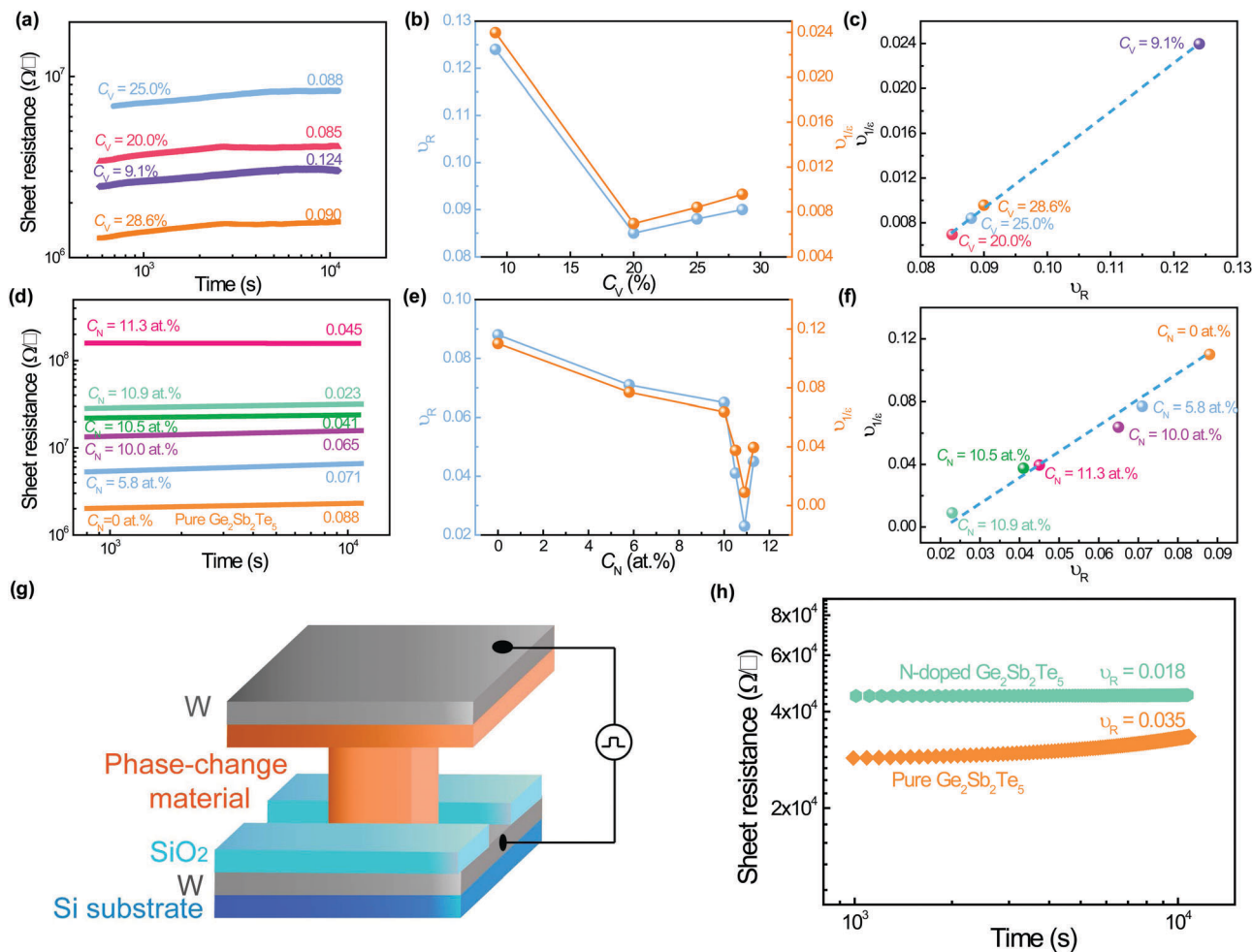
Fig. 2 (a) Sheet resistances of Ge–Sb–Te films at different vacancy concentrations as a function of annealing time at 50 °C. (b) ν_R and $\nu_{1/\varepsilon}$ as functions of vacancy concentration. (c) The linear relationship between ν_R and $\nu_{1/\varepsilon}$. (d) Sheet resistances of $Ge_2Sb_2Te_5$ films at different nitrogen contents as a function of annealing time at 50 °C. (e) ν_R and $\nu_{1/\varepsilon}$ as functions of nitrogen content. (f) The linear relationship between ν_R and $\nu_{1/\varepsilon}$. (g) The schematic diagram of a typical T-shaped cell structure. (h) Sheet resistance of two cells based on pure $Ge_2Sb_2Te_5$ ($C_N = 0$ at%) and N-$Ge_2Sb_2Te_5$ ($C_N = 10.9$ at%) films as a function of annealing time at 50 °C.

them (Fig. 2c) demonstrates again that resistance drift in phase-change films originates from the change in the reciprocal of the dielectric coefficient. The film with a vacancy concentration of 20.0% ($Ge_2Sb_2Te_5$) has the lowest ν_R due to the highest thermal stability of its dielectric coefficient (Fig. 2b). In previous studies, rigidity was generally considered as a major factor affecting the resistance drift.[32,41,46] Therefore, to analyze the reason for the variation of resistance drift, we measured the hardnesses and elastic moduli of the films with different vacancy concentrations before and after annealing. The results are shown in Fig. S7 (ESI†). As the vacancy concentration increases from 9.1% to 28.6%, the hardness and elastic modulus first increase and then decrease, and reached the maximum value when the vacancy concentration is 20%. The trend is in good agreement with the reciprocal of the dielectric coefficient, demonstrating that the observed decrease in the reciprocal of the dielectric coefficient is attributed to the introduction of vacancies leading to an increase in rigidity.

Considering that the $Ge_2Sb_2Te_5$ film with a vacancy concentration of 20.0% has the lowest ν_R, we further investigated the effect of nitrogen doping on its ν_R and $\nu_{1/\varepsilon}$. Fig. 2d shows that as the doped nitrogen content increases from 0 at% to 10.9 at%, the ν_R of the film decreases rapidly from 0.085 to 0.023, which is half of the best result (0.050) reported in the literature (Fig. 1b).[41] However, the ν_R increases to 0.045 as the doped nitrogen content further increases to 11.3 at%. The film containing 10.9 at% doped nitrogen has the lowest ν_R. This is because its dielectric coefficient is the most stable during annealing (Fig. 2e). These results indicate that proper nitrogen doping helps in reducing ν_R. Fig. 2f shows the linear relationship between $\nu_{1/\varepsilon}$ and ν_R, proving again that the relationship between $\nu_{1/\varepsilon}$ and ν_R obtained using the hydrogen-like model is correct. To further evaluate the resistance drift characteristics of pure $Ge_2Sb_2Te_5$ ($C_N = 0$ at%) and N-$Ge_2Sb_2Te_5$ ($C_N = 10.9$ at%) films in the device, we fabricated a device with a T-shaped structure (Fig. 2g). The sheet resistance of the cells as a

3390 | J. Mater. Chem. C, 2018, 6, 3387–3394

This journal is © The Royal Society of Chemistry 2018

Fig. 3 The SAED (top-left inset) and HRTEM images of pure $Ge_2Sb_2Te_5$ (C_N = 0 at%) (a) and N-$Ge_2Sb_2Te_5$ (C_N = 10.9 at%) films (b) annealed at 250 °C. (c) FTIR spectra of the as-deposited N-$Ge_2Sb_2Te_5$ films at different nitrogen contents. (d) The ratio between integrated intensities of Ge–N bonds in the annealed films and as-deposited ones at different nitrogen contents. The inset shows the FTIR spectra of the film with C_N = 11.3 at% before and after annealing at 50 °C.

function of annealing time is shown in Fig. 2h. Note that the ν_R of the pure $Ge_2Sb_2Te_5$ device is 0.035, whereas for the N-$Ge_2Sb_2Te_5$ (C_N = 10.9 at%) device it is 0.018. This is a 48.5% reduction, indicating that the introduction of nitrogen is an effective way to reduce resistance drift in both the material itself and the device.

To explore the reasons why nitrogen doping reduces the resistance drift and improves the thermal stability of the dielectric coefficient of the films, we studied the microstructures and chemical bonds of the films. Our XRD and SAED results (Fig. S8, ESI†) consistently indicate that $Ge_2Sb_2Te_5$ and N-$Ge_2Sb_2Te_5$ films are amorphous before annealing. However, the films transform into crystalline structures after annealing at 250 °C. Fig. 3a and b show the typical SAED and HRTEM images of the crystalline samples, where the cubic (111), (200) and (220) planes are labeled and periodic lattices are evident. Fig. 3c shows the FTIR spectra of the as-deposited films with different nitrogen contents. The peak intensity of the Ge–N bonds increases gradually with nitrogen content, indicating the formation of Ge–N bonds with N incorporation. Our XRD, SAED, HRTEM and FTIR results are in good agreement, which demonstrate that nitrogen doping does not change the original phase structure of the $Ge_2Sb_2Te_5$ films, but promote the formation of Ge–N bonds.

To reveal the effect of Ge–N bonds on the thermal stability of the dielectric coefficient of the film, we established two theoretical models: $Ge_2Sb_2Te_5$ and N-$Ge_2Sb_2Te_5$ (Fig. S9, ESI†). The density of states (DOS), electron density differences and modulus were calculated. Fig. 4b displays the DOS of the N-$Ge_2Sb_2Te_5$ model, wherein the overlap between Ge-4p and N-2p suggests the formation of covalent Ge–N bonds. Fig. 4c and d show that the density of charges between Ge and N atoms is higher than that between Ge and Te or Sb and Te atoms. This means that the

introduction of nitrogen leads to a significant increase in electron binding energy. Fig. 4e shows the calculated bulk and shear moduli before and after nitrogen doping. The bulk modulus increases from 40.5 to 49.9 GPa, and the shear modulus increases from 17.5 to 21.1 GPa with the introduction of nitrogen. Fig. 4f shows the measured elastic modulus and hardness of the films before and after nitrogen doping, wherein both the elastic modulus and the hardness increase with the introduction of nitrogen. These theoretical and experimental results are in good agreement, demonstrating that the formation of strong Ge–N bonds increases the rigidity of the network, which improves the thermal stability of the dielectric coefficient and thus reduces resistance drift significantly.

It is worth noting that the ν_R of the N-$Ge_2Sb_2Te_5$ films increases sharply when the nitrogen content is higher than 10.9 at% (Fig. 2d). This indicates that excessive N doping is unfavorable to the reduction of resistance drift. To understand this phenomenon, we measured the FTIR spectra of the films after annealing at 50 °C and calculated the ratios between integrated intensities of Ge–N bonds in the annealed films and the as-deposited ones (Fig. 3d). The ratio remains almost unchanged when the nitrogen content is less than 10.9 at%, indicating that thermal annealing does not destroy the Ge–N bonds. However, when the nitrogen content increases further to 11.3 at%, the ratio decreases significantly. This suggests that the nitrogen in $Ge_2Sb_2Te_5$ films with a high nitrogen content might escape[54,55] during annealing, leading to a decrease in Ge–N bonds. This greatly destroys the rigidity of the films, which leads to a decrease in the thermal stability of the dielectric coefficient and thus an increase in resistance drift.

We also studied the effect of nitrogen doping on the storage properties of the films in addition to the resistance drift. A lower decreasing rate (Fig. S10a, ESI†) and a wider temperature range (Fig. S10b, ESI†) for the intermediate resistance state are observed in nitrogen doped films, which favor the control of the intermediate resistance state and the improvement of the resolution of data read. The introduction of nitrogen not only increases the sheet resistance of amorphous and crystalline phases (Fig. S10c, ESI†), but also increases the crystallization temperature (from 170 to 210 °C, Fig. S10d, ESI†). According to $Q = I^2Rt$ (Q is the energy required to reset the PCM cell, I is the current, R is the crystalline resistance and t is the time), the increase of the crystalline resistance can substantially reduce the RESET current. Therefore, we believe that N doping can effectively reduce the power consumption of PCM devices. Researchers commonly believed that N doping induced resistance enhancement caused by the formation of Ge–N bonds between N and Ge, leading to grain refinement.[56–58] Indeed, our FTIR results (Fig. 3c) prove the formation of Ge–N bonds. The higher crystallization temperature indicates the improvement in thermal stability. These results show that the introduction of nitrogen effectively reduces resistance drift and at the same time improves the storage properties of phase-change films. This provides an effective way to prepare new phase-change films with high stability and high storage capacity.
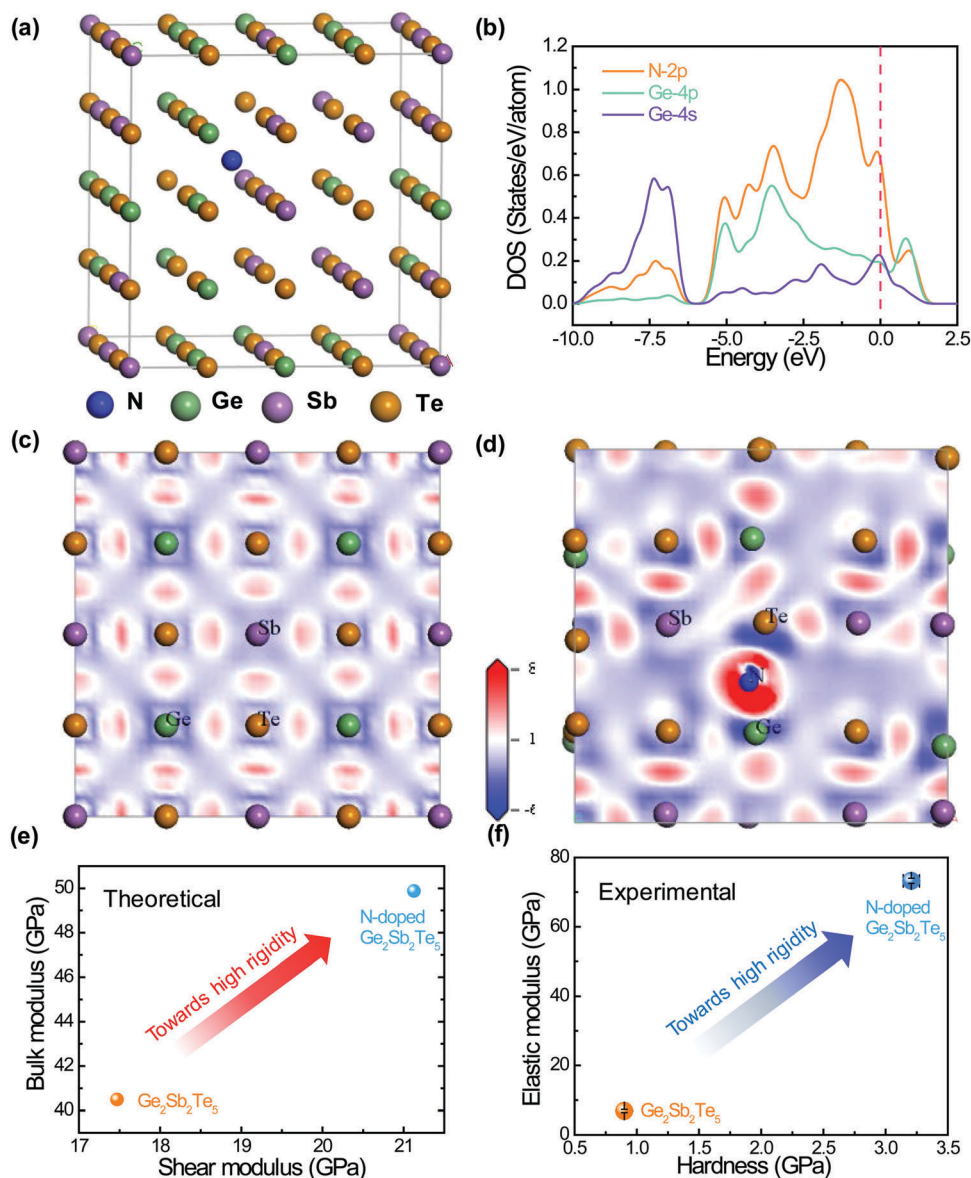
This journal is © The Royal Society of Chemistry 2018

J. Mater. Chem. C, 2018, 6, 3387–3394 | 3391

Fig. 4 (a) The model of N-Ge$_2$Sb$_2$Te$_5$. (b) The density of states of N-Ge$_2$Sb$_2$Te$_5$. The electron density difference before (c) and after (d) nitrogen doping. (e) The bulk and shear moduli of different structures obtained using first-principles calculation. (f) The measured elastic moduli and hardnesses of pure Ge$_2$Sb$_2$Te$_5$ (C_N = 0 at%) and N-Ge$_2$Sb$_2$Te$_5$ (C_N = 10.9 at%) films.

Conclusions

Using the hydrogen-like model, we find a proportional relationship between resistance drift and the reciprocal of the dielectric coefficient. The experimental results agree well with theoretical calculations, thus proving that the resistance drift in Ge–Sb–Te films originates from the change in the dielectric coefficient caused by structural relaxation. On the basis of its microscopic origin, we proposed a new strategy to reduce resistance drift in phase-change films: improving the thermal stability of the dielectric coefficient. Two validation experiments prove that our strategy is very effective. Both vacancy incorporation and nitrogen doping improve the thermal stability of the dielectric coefficient of Ge–Sb–Te films. With a combination of vacancy incorporation and nitrogen doping, the resistance drift exponent

decreases to 0.023, which is lower by half than the best result (0.050) reported in the literature. At the same time, the storage properties of the film are also improved. Therefore, the stability and storage function of phase-change films can be simultaneously improved by modification of their dielectric properties. This opens a new door for the development of film materials for MLC PCM.

Experimental

Film deposition

Pure Ge–Sb–Te films were prepared using RF magnetron sputtering systems. Ge$_8$Sb$_2$Te$_{11}$, Ge$_2$Sb$_2$Te$_5$, Ge$_1$Sb$_2$Te$_4$, and Ge$_1$Sb$_4$Te$_7$ films were deposited on silicon and glass wafers in Ar by sputtering Ge$_8$Sb$_2$Te$_{11}$, Ge$_2$Sb$_2$Te$_5$, Ge$_1$Sb$_2$Te$_4$, and Ge$_1$Sb$_4$Te$_7$ targets, respectively.

3392 | J. Mater. Chem. C, 2018, 6, 3387–3394

This journal is © The Royal Society of Chemistry 2018

The distance between the target and substrate holder, starting pressure, working pressure, sputtering power, substrate temperature and deposition time were 55 mm, 4×10^{-4} Pa, 0.6 Pa, 60 W, 25 °C, and 25 min, respectively. The vacancy concentrations of $Ge_8Sb_2Te_{11}$, $Ge_2Sb_2Te_5$, $Ge_1Sb_2Te_4$, and $Ge_1Sb_4Te_7$ were 9.09%, 20%, 25%, and 28.6%, respectively, calculated by

$$C_V = \frac{n(Te) - n(Ge) - n(Sb)}{n(Te)} \times 100\%,$$

where n(Ge), n(Sb), and n(Te) were the corresponding stoichiometric numbers.

Nitrogen-doped $Ge_2Sb_2Te_5$ films were prepared using RF magnetron sputtering systems in mixed discharge gases of Ar and N_2. The distance between the target and substrate holder, starting pressure, working pressure, sputtering power, substrate temperature and deposition time were 55 mm, 4×10^{-4} Pa, 0.6 Pa, 60 W, 25 °C, and 25 min, respectively. During the deposition, the flow rates of Ar and N_2 were accurately controlled by independent mass flow controllers. Films with different N contents were obtained by changing the $N_2/(Ar + N_2)$ flow ratio from 0 to 2.1%.

T-shaped device cell preparation

A T-shaped device cell was fabricated using an ultraviolet exposure system (MDA-400M) based on lift-off technology[59–61] and magnetron sputtering. For details, see Section VI of the ESI.†

Sample characterization

The microstructure of the films was characterized by X-ray Diffraction (XRD) using a Bruker D8Tools X-ray diffractometer, Selected Area Electron Diffraction (SAED) and High-Resolution Transmission Electron Microscopy (HRTEM, JEOL TEM-2010). The elemental composition of the films was analyzed using a scanning electron microscope (SEM, SU8010, HITACHI, Japan) equipped with an energy dispersive spectrometer (EDX) and an X-ray photoelectron spectrometer (XPS, ESCALAB 250 Thermo Electron, USA). A Fourier Transform Infrared spectrometer (FTIR, Spectrum One B, Perkin Elmer, USA) was used to measure the infrared absorption spectra. The transmission spectra between 300 nm and 2500 nm were measured using a UV-VIS-NIR spectrometer (Lambda 900, Perkin Elmer, USA). According to the envelope method,[62] we calculated the refractive index n and the absorption coefficient α.[63,64] The dielectric coefficient was derived from the formula $\varepsilon = n^2$, and the optical band gap was calculated by the Tauc method.[65] For details, see Section VII of the ESI.† A four-point probe system was used to measure the sheet resistances for different annealing times at an annealing temperature of 50 °C.

First-principles calculation

The electronic structures of pure $Ge_2Sb_2Te_5$ and N-$Ge_2Sb_2Te_5$ were calculated using the CASTEP package based on Density Functional Theory.[33,66] The generalized gradient approximation (GGA) with the Perdew–Burke–Ernzerhof (PBE) parameterization was used to express the exchange–correlation energy of interacting electrons. For details, see Section IV of the ESI.†

Conflicts of interest

There are no conflicts to declare.

Acknowledgements

Notes and references

1 N. Przulj and N. Malod-Dognin, *Science*, 2016, **353**, 123–124.
2 J. U. Adams, *Nature*, 2015, **527**, S108–S109.
3 G. Y. Jia, G. J. Han, J. F. Jiang and L. Liu, *IEEE T. Ind. Inform.*, 2017, **13**, 1951–1960.
4 D. Lencer, M. Salinga, B. Grabowski, T. Hickel, J. Neugebauer and M. Wuttig, *Nat. Mater.*, 2008, **7**, 972–977.
5 K. Shportko, S. Kremers, M. Woda, D. Lencer, J. Robertson and M. Wuttig, *Nat. Mater.*, 2008, **7**, 653–658.
6 M. Wuttig and N. Yamada, *Nat. Mater.*, 2007, **6**, 824–832.
7 P. N. Bartlett, S. L. Benjamin, C. H. de Groot, A. L. Hector, R. M. Huang, A. Jolleys, G. P. Kissling, W. Levason, S. J. Pearce, G. Reid and Y. D. Wang, *Mater. Horiz.*, 2015, **2**, 420–426.
8 E. Pallecchi, Z. Chen, G. E. Fernandes, Y. Wan, J. H. Kim and J. Xu, *Mater. Horiz.*, 2015, **2**, 125–129.
9 R. E. Simpson, P. Fons, A. V. Kolobov, T. Fukaya, M. Krbal, T. Yagi and J. Tominaga, *Nat. Nanotechnol.*, 2011, **6**, 501–505.
10 J. Kalikka, X. L. Zhou, E. Dilcher, S. Wall, J. Li and R. E. Simpson, *Nat. Commun.*, 2016, **7**, 11983.
11 K. K. Du, Q. Li, Y. B. Lyu, J. C. Ding, Y. Lu, Z. Y. Cheng and M. Qiu, *Light: Sci. Appl.*, 2017, **6**, e16194.
12 J. Tominaga, R. E. Simpson, P. Fons and A. V. Kolobov, *Appl. Phys. Lett.*, 2011, **99**, 152105.
13 X. Yu and J. Robertson, *Sci. Rep.*, 2016, **6**, 37325.
14 S. R. Elliott, *Int. J. Appl. Glass Sci.*, 2015, **6**, 15–18.
15 T. H. Lee and S. R. Elliott, *Adv. Mater.*, 2017, **29**, 1700184.
16 X. Zhou, J. Kalikka, X. Ji, L. Wu, Z. Song and R. E. Simpson, *Adv. Mater.*, 2016, **28**, 3007–3016.
17 J. M. Skelton, D. Loke, T. Lee and S. R. Elliott, *ACS Appl. Mater. Interfaces*, 2015, **7**, 14223–14230.
18 M. Krbal, A. V. Kolobov, P. Fons, K. V. Mitrofanov, Y. Tamenori, J. Hegedüs, S. R. Elliott and J. Tominaga, *Appl. Phys. Lett.*, 2013, **102**, 111904.
19 R. E. Simpson, M. Krbal, P. Fons, A. V. Kolobov, J. Tominaga, T. Uruga and H. Tanida, *Nano Lett.*, 2010, **10**, 414–419.
20 A. Athmanathan, M. Stanisavljevic, N. Papandreou, H. Pozidis and E. Eleftheriou, *IEEE J. Em. Sel. Top. C*, 2016, **6**, 87–100.
21 A. Gokce, I. Cinar, S. C. Ozdemir, E. Cogulu, B. Stipe, J. A. Katine and O. Ozatay, *IEEE Trans. Electron Devices*, 2016, **63**, 3103–3108.
22 W. S. Khwa, M. F. Chang, J. Y. Wu, M. H. Lee, T. H. Su, T. Y. Wang, H. P. Li, M. BrightSky, S. Kim, H. L. Lung and C. Lam, *IEEE Electron Device Lett.*, 2016, **37**, 1422–1425.
23 S. Kim, N. Sosa, M. BrightSky, D. Mori, W. K. Kim, Y. Zhu, K. K. Suu and C. Lam, *IEEE Trans. Electron Devices*, 2016, **63**, 3922–3927.

This journal is © The Royal Society of Chemistry 2018

J. Mater. Chem. C, 2018, **6**, 3387–3394 | 3393

24 M. Krbal, A. V. Kolobov, P. Fons, J. Tominaga, S. R. Elliott, J. Hegedus, A. Giussani, K. Perumal, R. Calarco, T. Matsunaga, N. Yamada, K. Nitta and T. Uruga, *Phys. Rev. B: Condens. Matter Mater. Phys.*, 2012, **86**, 045212.

25 X. Zhou, J. K. Behera, S. Lv, L. Wu, Z. Song and R. E. Simpson, *Nano Futur.*, 2017, **1**, 025003.

26 J. Tominaga, Y. Saito, K. Mitrofanov, N. Inoue, P. Fons, A. V. Kolobov, H. Nakamura and N. Miyata, *Adv. Funct. Mater.*, 2017, 1702243.

27 H. Lu, E. Thelander, J. W. Gerlach, U. Decker, B. Zhu and B. Rauschenbach, *Adv. Funct. Mater.*, 2013, **23**, 3621–3627.

28 J. Y. Raty, W. Zhang, J. Luckas, C. Chen, R. Mazzarello, C. Bichara and M. Wuttig, *Nat. Commun.*, 2015, **6**, 7467.

29 D. Krebs, T. Bachmann, P. Jonnalagadda, L. Dellmann and S. Raoux, *New J. Phys.*, 2014, **16**, 043015.

30 F. Dirisaglik, G. Bakan, Z. Jurado, S. Muneer, M. Akbulut, J. Rarey, L. Sullivan, M. Wennberg, A. King, L. Zhang, R. Nowak, C. Lam, H. Silva and A. Gokirmak, *Nanoscale*, 2015, **7**, 16625–16630.

31 M. Rutten, M. Kaes, A. Albert, M. Wuttig and M. Salinga, *Sci. Rep.*, 2015, **5**, 17362.

32 A. A. Piarristeguy, M. Micoulaut, R. Escalier, P. Jovari, I. Kaban, J. van Eijk, J. Luckas, S. Ravindren, P. Boolchand and A. Pradel, *J. Chem. Phys.*, 2015, **143**, 074502.

33 J. Tominaga, A. V. Kolobov, P. Fons, T. Nakano and S. Murakami, *Adv. Mater. Interfaces*, 2014, **1**, 1300027.

34 M. Rizzi, A. Spessot, P. Fantini and D. Ielmini, *Appl. Phys. Lett.*, 2011, **99**, 223513.

35 P. Fantini, S. Brazzelli, E. Cazzini and A. Mani, *Appl. Phys. Lett.*, 2012, **100**, 013505.

36 K. Hosotani, Y. Asao, M. Nagamine, T. Ueda, F. Aikawa, N. Shimomura, S. Ikegawa, T. Kajiyama, S. Takahashi, A. Nitayama and H. Yoda, *IEEE Int. Reliab. Phys. Symp. Proc.*, 2007, 650.

37 S. Kim, B. Lee, M. Asheghi, F. Hurkx, J. P. Reifenberg, K. E. Goodson and H. S. P. Wong, *IEEE Trans. Electron Devices*, 2011, **58**, 584–592.

38 A. Kiouseloglou, G. Navarro, V. Sousa, A. Persico, A. Roule, A. Cabrini, G. Torelli, S. Maitrejean, G. Reimbold, B. De Salvo, F. Clermidy and L. Perniola, *IEEE Trans. Electron Devices*, 2014, **61**, 1246–1254.

39 G. Betti Beneventi, L. Perniola, V. Sousa, E. Gourvest, S. Maitrejean, J. C. Bastien, A. Bastard, B. Hyot, A. Fargeix, C. Jahan, J. F. Nodin, A. Persico, A. Fantini, D. Blachier, A. Toffoli, S. Loubriat, A. Roule, S. Lhostis, H. Feldis, G. Reimbold, T. Billon, B. De Salvo, L. Larcher, P. Pavan, D. Bensahel, P. Mazoyer, R. Annunziata, P. Zuliani and F. Boulanger, *Solid-State Electron.*, 2011, **65-66**, 197–204.

40 J. Luckas, D. Krebs, S. Grothe, J. Klomfaß, R. Carius, C. Longeaud and M. Wuttig, *J. Mater. Res.*, 2013, **28**, 1139–1147.

41 J. Luckas, A. Olk, P. Jost, H. Volker, J. Alvarez, A. Jaffré, P. Zalden, A. Piarristeguy, A. Pradel, C. Longeaud and M. Wuttig, *Appl. Phys. Lett.*, 2014, **105**, 092108.

42 M. Wimmer, M. Kaes, C. Dellen and M. Salinga, *Front. Phys.*, 2014, **2**, 75.

43 J. E. Boschker, M. Boniardi, A. Redaelli, H. Riechert and R. Calarco, *Appl. Phys. Lett.*, 2015, **106**, 023117.

44 S. Gabardi, S. Caravati, G. C. Sosso, J. Behler and M. Bernasconi, *Phys. Rev. B: Condens. Matter Mater. Phys.*, 2015, **92**, 054201.

45 J. Y. Cho, T. Y. Yang, Y. J. Park and Y. C. Joo, *Electrochem. Solid-State Lett.*, 2012, **15**, H81.

46 F. Zipoli, D. Krebs and A. Curioni, *Phys. Rev. B*, 2016, **93**, 115201.

47 A. A. Piarristeguy, M. Micoulaut, R. Escalier, P. Jovari, I. Kaban, J. van Eijk, J. Luckas, S. Ravindren, P. Boolchand and A. Pradel, *J. Chem. Phys.*, 2015, **143**, 074502.

48 W. W. Koelmans, A. Sebastian, V. P. Jonnalagadda, D. Krebs, L. Dellmann and E. Eleftheriou, *Nat. Commun.*, 2015, **6**, 8181.

49 D. Ielmini, S. Lavizzari, D. Sharma and A. L. Lacaita, *IEEE Int. Electron Devices Meet.*, 2007, **1**(2), 939–942.

50 H. Haug and S. W. Koch, *Quantum Theory of the Optical and Electronic Properties of Semiconductors*, World Scientific, Singapore, 1990.

51 P. E. D. J. Griffiths and D. Kindersley, *Introduction to Electrodynamics*, 1962.

52 J. J. Zhao, F. R. Liu, X. X. Han, N. Bai, Y. H. Wan, X. Lin and F. Liu, *Appl. Surf. Sci.*, 2014, **289**, 160–166.

53 Y.-J. Chen, B. Zhang, Q.-Q. Ding, Q.-S. Deng, Y. Chen, Z.-T. Song, J.-X. Li, Z. Zhang and X.-D. Han, *J. Alloys Compd.*, 2016, **678**, 185–192.

54 K. Kim, J.-C. Park, J.-G. Chung, S. A. Song, M.-C. Jung, Y. M. Lee, H.-J. Shin, B. Kuh, Y. Ha and J.-S. Noh, *Appl. Phys. Lett.*, 2006, **89**, 243520.

55 Z. Sun, J. Zhou, H.-J. Shin, A. Blomqvist and R. Ahuja, *Appl. Phys. Lett.*, 2008, **93**, 241908.

56 L. Cheng, L. Wu, Z. Song, F. Rao, C. Peng, D. Yao, B. Liu and L. Xu, *J. Appl. Phys.*, 2013, **113**, 044514.

57 B. Huang, *Phys. Status Solidi B*, 2015, **252**, 431–441.

58 Z. Xu, B. Liu, Y. Chen, Z. Zhang, D. Gao, H. Wang, Z. Song, C. Wang, J. Ren, N. Zhu, Y. Xiang, Y. Zhan and S. Feng, *Solid-State Electron.*, 2016, **116**, 119–123.

59 L. Alloatti, R. Palmer, S. Diebold, K. P. Pahl, B. Chen, R. Dinu, M. Fournier, J.-M. Fedeli, T. Zwick, W. Freude, C. Koos and J. Leuthold, *Light: Sci. Appl.*, 2014, **3**, e173.

60 S. Schuhladen, K. Banerjee, M. Stürmer, P. Müller, U. Wallrabe and H. Zappe, *Light: Sci. Appl.*, 2016, **5**, e16005.

61 K. Lee, J. Lee, B. A. Mazor and S. R. Forrest, *Light: Sci. Appl.*, 2015, **4**, e288.

62 R. Swanepoel, *J. Phys. E: Sci. Instrum.*, 1983, **16**, 1214.

63 S. Saeed, C. de Weerd, P. Stallinga, F. C. M. Spoor, A. J. Houtepen, L. Da Siebbeles and T. Gregorkiewicz, *Light: Sci. Appl.*, 2015, **4**, e251.

64 J. Guo, J.-J. Xie, D.-J. Li, G.-L. Yang, F. Chen, C.-R. Wang, L.-M. Zhang, Y. M. Andreev, K. A. Kokh, G. V. Lanskii and V. A. Svetlichnyi, *Light: Sci. Appl.*, 2015, **4**, e362.

65 Z. Liu, F. Huang, H. Huang, S. Zhang, K. Zhang, W. Zheng and C. Hu, *Vacuum*, 2017, **141**, 32–40.

66 J. Hegedus and S. R. Elliott, *Nat. Mater.*, 2008, **7**, 399–405.

3394 | *J. Mater. Chem. C*, 2018, **6**, 3387–3394

This journal is © The Royal Society of Chemistry 2018